Acta Materialia 126 (2017) 202–209

Contents lists available at ScienceDirect

Acta Materialia

journal homepage: www.elsevier.com/locate/actamat

Full length article

Small-volume aluminum alloys with native oxide shell deliver unprecedented strength and toughness

Shi-Hao Li [a], Wei-Zhong Han [a, *], Ju Li [a, b], Evan Ma [a, c], Zhi-Wei Shan [a]

[a] Center for Advancing Materials Performance from the Nanoscale (CAMP-Nano) & Hysitron Applied Research Center in China (HARCC), State Key Laboratory for Mechanical Behavior of Materials, Xi'an Jiaotong University, Xi'an, 710049, China
[b] Department of Nuclear Science and Engineering and Department of Materials Science and Engineering, Massachusetts Institute of Technology, Cambridge, MA, 02139, USA
[c] Department of Materials Science and Engineering, Johns Hopkins University, Baltimore, MD, 21218, USA

ARTICLE INFO

Article history:
Received 23 June 2016
Received in revised form
2 October 2016
Accepted 20 December 2016

Keywords:
Aluminum
Native oxide shell
Small-volume metals
Strength
Toughness

ABSTRACT

Mechanically robust nanoscale metallic materials are highly desirable in many miniaturized devices. However, the lack of strain hardening and controllable plasticity plagues such small-volume metals. Using Al-4Cu alloy as an example, here we show that a submicron-sized metallic material with ultrathin native oxide shell exhibits a high degree of deformation controllability, unprecedented strain hardening, size strengthening and toughness, in uniaxial tensile deformation. The metal/native oxide "composite" is easy to make, and the emergent properties extend well beyond the benchmark range known for metals in a normalized (i.e., dimensionless) strength-toughness plot. The origin of the combination of strengthening and plastic stability is that an intact ultrathin native oxide shell exerts a strong confinement on dislocation movement and annihilation, thereby breaking the envelope on dislocation storage and strain hardening achievable in small-volume metals.

1. Introduction

Mechanical properties of small volume metals have attracted tremendous interests in the past decade due to potential microscale and nanoscale applications [1,2]. A variety of metals and alloys were fabricated into micro- and nanoscale samples, and tested under micro-compression or tension, in order to explore their size-strength relationship [1–12]. A strong sample size-dependent strength behavior has been reported for small-volume metals, hence the phrase "smaller is stronger". "Dislocation starvation" [6,7] and "truncation of dislocation sources" [8–10] theories have been proposed to explain the dislocation-avalanche-controlled jerky flow and the size-dependent strengthening. However, some unfavorable deformation characters, such as strain bursts, lack of strain hardening and near-zero uniform elongation, are often displayed by the small volume metals [1–12]. Therefore, how to overcome the deformation instability, lack of strain hardening and strength-ductility tradeoff still remains as a bottleneck for the utilization of microscale and nanoscale metals.

Recently, interfaces [13–19], precipitates [20–25] and artificially deposited thin film cover [26,27] have been introduced into small volume metals to amend the deformation instability. These attempts show improved deformation stability, but strain bursts are still frequently observed, and meanwhile the strain hardening is still very limited due to the inefficiency of dislocation storage [17–25]. In this regard, new strategies need to be developed. Here we report that the naturally formed ultrathin native oxide shell could promote efficient storage of dislocations in a small-volume Al-4Cu alloy, thus effectively suppressing strain bursts and enhancing strain hardening. As a result, the nanoscale Al-4Cu alloys demonstrate high degree of deformation controllability, unprecedented strain hardening, size strengthening, and extraordinary combination of strength and toughness, showing a broad spectrum of mechanical performances that are superior to other small-volume metals [1–12] (as well as their bulk counterparts).

2. Experimental design

We choose Al-4Cu alloy aged at 200 °C for 1.5 h (peak aged) as the model material. It contains a high density of shear-resistant precipitates, θ' (Al_2Cu) [28,29]. The plate-shaped shear-resistant precipitates form on $\{001\}_\alpha$ planes of the Al matrix. As shown in

* Corresponding author.
E-mail address: wzhanxjtu@mail.xjtu.edu.cn (W.-Z. Han).

http://dx.doi.org/10.1016/j.actamat.2016.12.055
1359-6454/

Fig. 1a and 1b, two edge-on variants of precipitates and one face-on variant precipitate can be observed with the electron beam along the $<001>_{\alpha}$ in transmission electron microscope (TEM). The interface structure of θ' and Al matrix can be found elsewhere [30]. The average grain sizes of the peak aged Al-4Cu are ~80 μm, hence it is easy to cut out nanoscale single crystal samples, away from grain boundaries for nano-mechanical testing. Micro-tensile samples with size, $D(D \equiv \sqrt{A}$, where A is the cross-section area of tensile samples), ranging from 100 nm to 800 nm were fabricated by focused ion beam (FIB) micromachining. The final polishing was done using a low ion beam current to minimize possible Ga^{+} damage. Quantitative *in situ* mechanical tests were conducted using a Hysitron PicoIndentor (PI95) inside a FEG JEOL 2100F TEM (200 kV) under displacement control. The displacement rate was programmed to be 5 nm/s in tension, which corresponds to a strain rate of $\sim 5 \times 10^{-3}\ s^{-1}$. In order for easy comparison, all of the tensile tests were performed using the fixed strain rate of $5 \times 10^{-3}\ s^{-1}$ in current study. Tensile samples with various sizes were loaded along four different orientations ([100], [$\bar{3}$11], [$\bar{7}$40] and [$\bar{1}$10]). Real-time observation of the tensile deformation was recorded by a charge-coupled device camera. All tensile samples were examined in SEM and TEM to determine the sample sizes and loading axis before *in situ* tensile tests.

3. Results

3.1. Size-dependent tensile properties

Fig. 1a shows a typical Al-4Cu single crystal micro-tensile sample. Profuse plate-shaped θ' precipitates can be found in the small volume inside the single crystal. These precipitates have habit planes along $\{001\}_{Al}$, as highlighted in Fig. 1b. The average precipitates length and thickness are 56 ± 20 nm and 2.3 nm, respectively [28]. The total volume fraction of θ' is ~2.6%. Besides, a layer of ultrathin and fully dense native amorphous Al oxide shell, with a homogeneous thickness of $<t> = 4.3$ nm, covers the whole micro-tensile sample, as displayed in Fig. 1c. Such a native Al oxide film is typical for Al alloys once exposed to air [31–33]. The thickness of the native Al oxide film is roughly the same for all the tensile sample dimensions.

Fig. 1d (red curve) demonstrates the tensile true stress-strain curve of an Al-4Cu single crystal with $D = 245$ nm and loading along [$\bar{3}$11]. With increasing stress, the nanoscale Al-4Cu single crystal shows linear elastic behavior, and yields at ~0.68 GPa, following a steep, stable and continuous strain hardening up to the ultimate tensile strength (UTS) of ~1 GPa, then fractured with a total strain of ~13%. No strain burst or jerky flow was displayed during tension, significantly different from the unstable deformation of other small-volume metals [1–12]. For comparison, we also tested a pure Al single crystal sample with native Al oxide shell. The sample had a similar size ($D = 255$ nm) but was loaded along [$\bar{1}$10], as shown in Fig. 1d (blue curve) and Movie S1. The nanoscale Al single crystal shows a similar yield strength as the nanoscale Al-4Cu. However, there is only a very short stable deformation and strain hardening stage after yielding, showing a serrated stress-strain response, although the strain burst is much smaller than previously reported [1–12]. As revealed by Movie S1, the jerky flow in the nanoscale Al case mainly results from the dislocation-native

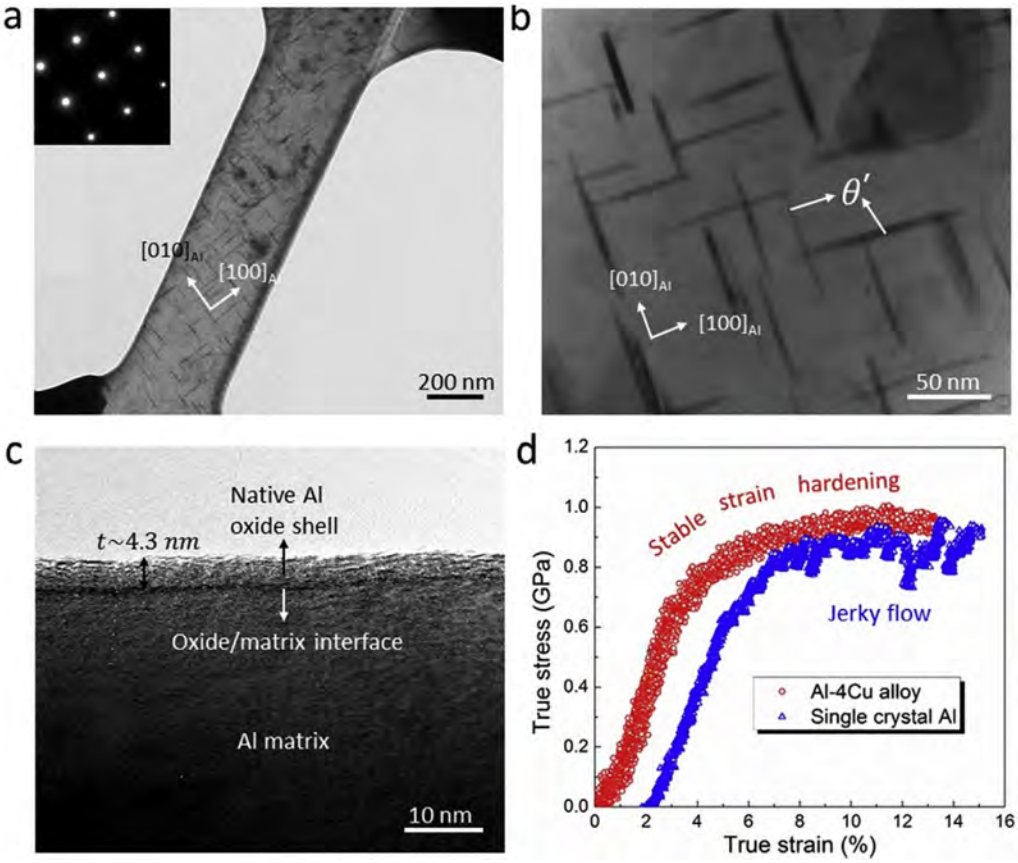

Fig. 1. Microstructure and tensile deformation of nanoscale Al and Al-4Cu. **(a)** TEM image of Al-4Cu single crystal tensile sample. The inserted is the selected area diffraction pattern of $[001]_{Al}$; **(b)** Highlight of the shear-resistant precipitates (θ') in Al matrix; **(c)** A layer of fully dense and ultrathin native Al oxide shell with thickness of 4.3 nm is formed on the Al and Al-4Cu sample; **(d)** True stress-strain curves of a nanoscale Al-4Cu single crystal (red curve, $D = 245$ nm) and an Al single crystal (blue curve, $D = 255$ nm). (For interpretation of the references to colour in this figure legend, the reader is referred to the web version of this article.)

oxide shell interactions: once dislocations break apart the oxide shell in a local region, a tiny strain burst appears on the stress strain curve (Fig. 1d). The difference between the Al-4Cu and Al cases indicates that an intact native oxide shell plays a dominate role in contributing to the stable plastic flow, while the θ' precipitates can reduce the shear localization and further improve the deformation stability. A quantification of the deformation stability according to mechanical controllability index (MCI) [15] found that, nanoscale Al-4Cu has an index of MCI = 7, which is much higher than the nanocrystalline Al pillar (MCI = 4) and single crystal Al pillar (MCI = 0.33) [15] under compression.

Supplementary video related to this article can be found at http://dx.doi.org/10.1016/j.actamat.2016.12.055.

To explore the size strengthening of nanoscale Al-4Cu alloy, more than 30 micro-tensile tests were performed with D ranging from 100 nm to 800 nm. Fig. 2a shows three typical true stress-strain curves of Al-4Cu single crystals with D = 131 nm, 282 nm and 733 nm, in comparison with bulk polycrystalline Al-4Cu. With reducing sample dimension, the true stress strain curves become steeper and steeper, and the elastic modulus, yield strength and strain hardening increase significantly. The yield strength at D = 733 nm is ~0.32 GPa, analogous to the bulk Al-4Cu. While the yield strength increased markedly with reducing sample dimension, and reached ~0.9 GPa for the sample with D = 131 nm. Notably, the UTS of Al-4Cu with D = 733 nm is 0.52 GPa, only ~60% increase compared to its yield strength. In comparison, the UTS of Al-4Cu with D = 131 nm is 1.9 GPa, a ~110% increase, indicating significant size-dependent strain hardening, as shown in Fig. 2a. Fig. 2b displays the variation of the strain hardening rate of nanoscale Al-4Cu as a function of strain, for samples shown in Fig. 2a and in comparison with bulk Al-4Cu. A trend of "smaller is higher strain hardening" can be identified, and the variation of strain hardening rate with strain is much steeper for samples with smaller dimension. Obviously, the initial strain hardening rate of nanoscale Al-4Cu is roughly an order of magnitude higher than bulk Al-4Cu (Fig. 2b). In order to quantify the size-dependent strengthening, the yield stress and UTS were quantified and summarized in Fig. 2c and d. A clear trend of smaller is stronger can be identified for nanoscale Al-4Cu alloys. With increasing sample dimension, both the yield strength and UTS are trending to reach the level of bulk sample, as shown in Fig. 2c and d. In addition, the strength of nanoscale Al-4Cu alloys is not sensitive to the loading axes (Fig. 2c and d), which is likely due to the effect of ultrathin native oxide shell and shear-resistant precipitates that can alleviate the mechanical anisotropy.

Fig. 3a summarizes the variation of yield strength of nanoscale Al-4Cu with its sample dimension D, roughly two stages size dependent strengthening can be identified at D = 250 nm according to the log-log plot. For D > 250 nm, a weak size-dependent strengthening with size strengthening factor (m) of 0.29 can be measured and labelled as stage I (Fig. 3a). However, for D < 250 nm, a steeper size-dependent strengthening stage is displayed by the nanoscale Al-4Cu with m = 0.90, and marked as stage II. This phenomenon is anomalous because the precipitates contained micro pillars usually demonstrate a size-independent strengthening due to the constant precipitate spacing [20–22]. Similarly, the UTS of nanoscale Al-4Cu demonstrates a strong size-dependent behavior as well, as shown in Fig. 3b. For D > 250 nm, a slow increasing of UTS with sample size with m = 0.33 was observed, and labelled as stage I. Once D < 250 nm, a quick increasing of UTS with sample dimension with m = 1.07 can be identified, marked as stage II. The current ultrahigh size strengthening factor of 1.07 is almost the highest value reported for nanoscale Al pillars so far

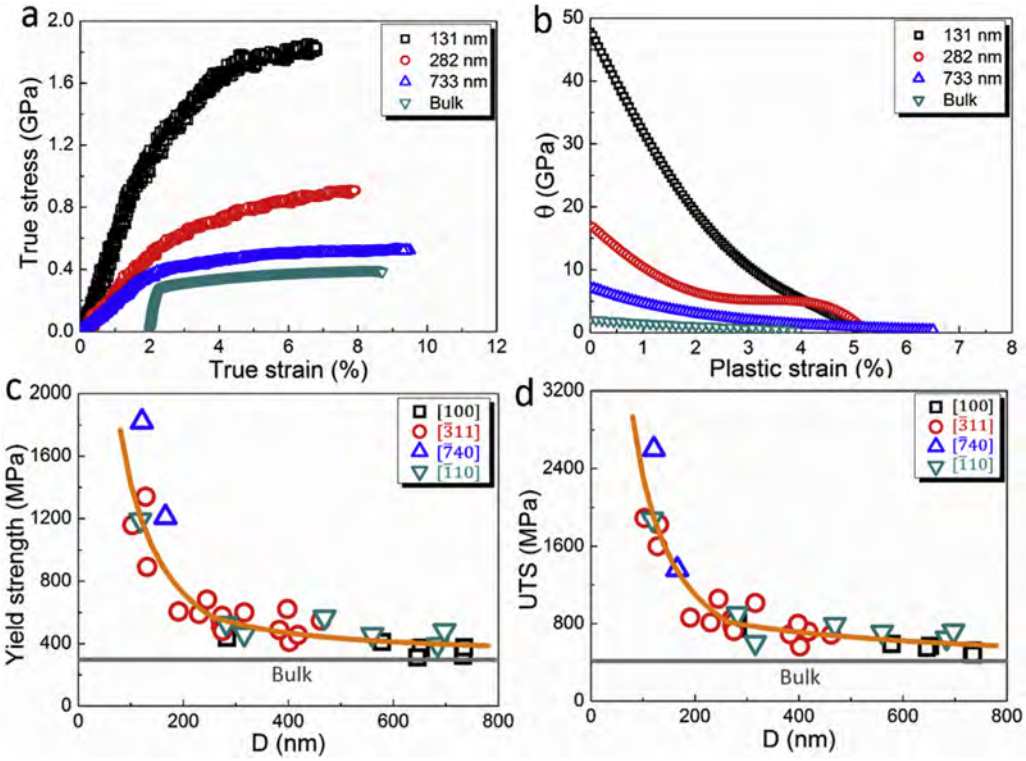

Fig. 2. Size-dependent tensile deformation of nanoscale Al-4Cu. **(a)** True stress-strain curves of nanoscale Al-4Cu with D = 131 nm (black curve), D = 282 nm (red curve), D = 733 nm (blue curve) and bulk Al-4Cu; **(b)** Strain hardening plot of true stress-strain curves shown in (a); **(c)** Yield strength and **(d)** UTS of nanoscale Al-4Cu vary with the sample sizes. Both yield strength and UTS are not sensitive to loading orientations. The stress strain curve of bulk sample in (a) is shifted for legibility. The yellow line in (c) is model prediction. (For interpretation of the references to colour in this figure legend, the reader is referred to the web version of this article.)

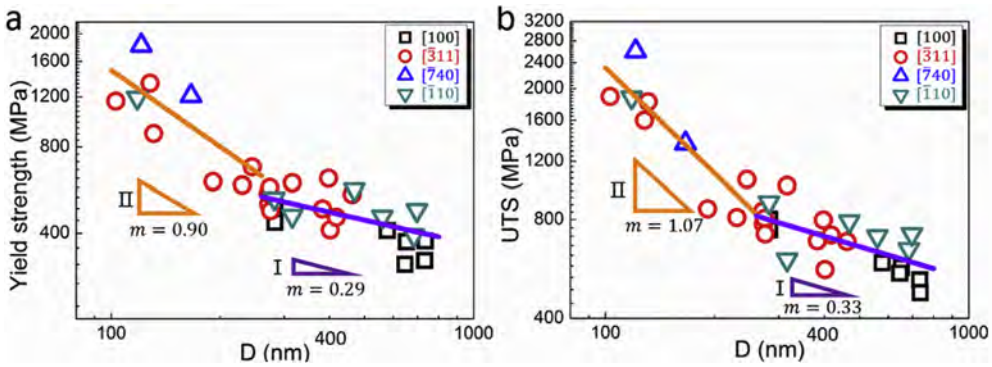

Fig. 3. The variation of yield strength **(a)** and UTS **(b)** of nanoscale Al-4Cu vary with the sample sizes. Both yield strength and UTS are not sensitive to loading orientations. Two size dependent stages can be divided at $D = 250$ nm according to the log-log plots.

[4,12,13,15].

3.2. Dislocation storage and size-dependent fracture

To understand the anomalous size-dependent strengthening and strain hardening displayed by the nanoscale Al-4Cu alloy, the dislocation structure evolution during straining was investigated in detail. Fig. 4a and Movie S2 show the evolution of dislocation structures in the micro-tensile test of an Al with $D = 200$ nm. Before straining, the interior of the Al tensile sample was roughly clean (Fig. 4a-I). When strain increased to ~7.1%, some dislocations start to accumulate in the lower part of the tensile sample, especially along the sample edges, as marked by the red arrows in Fig. 4a-II. Further elevating the strain to 12.5%, more and more dislocations are stored inside the nanoscale Al, and a slightly higher number of dislocations distribute along the edges of sample (Fig. 4a-III). Such a behavior of dislocation accumulation is pretty similar to a previous report on the tensile deformation of micron-sized Al fibers [12]. Once the sample fractured, these previously accumulated dislocations were released quickly at the point of fracture (Fig. 4a-IV), indicating the critical role of an intact native Al oxide shell in assisting dislocation storage. The number of dislocation accumulated was difficult to count due to the dynamic loading and improper viewing orientation. Fig. 4b and Movie S3 demonstrate the evolution of dislocation structures in the nanoscale Al-4Cu during *in situ* tensile test. In contrast to the Al case, with gradually increasing strain from 0 to 8.2%, dislocations start to accumulate both around θ' precipitates and at the sample edges (Fig. 4b-II). Further elevating the strain to 12.1%, dislocations increased quickly across the sample, mostly distributed around the θ' precipitates and partly piled up along the edges, as shown in Fig. 4b-III. After fracture, a large fraction of the accumulated dislocations were remained inside the sample, indicating the important role of θ' precipitates in stabilizing the dislocations, as displayed in Fig. 4-IV. From the comparison between Al and Al-4Cu, it is evident that the native Al oxide shell and θ' precipitates play critical roles in assisting dislocation storage, and leading to the significant strain hardening.

Supplementary video related to this article can be found at http://dx.doi.org/10.1016/j.actamat.2016.12.055.

The nanoscale Al-4Cu samples show a clear transition from elastic to plastic deformation, stable flow stress and significant strain hardening. Such a bulk-like tensile deformation character provides opportunity for us to investigate the uniform elongation of nanoscale samples, which was impossible in the strain burst dominated single crystal pillars [1–12]. The uniform elongation of

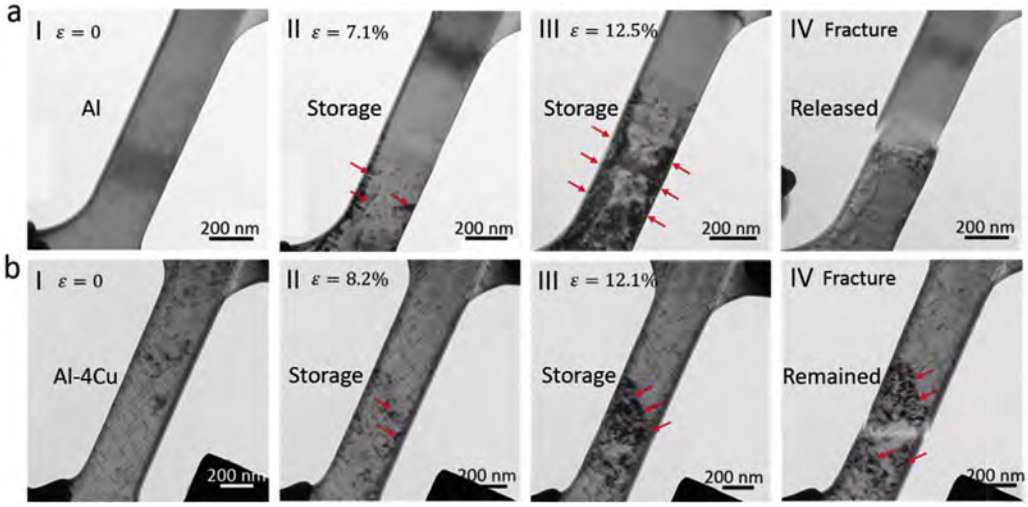

Fig. 4. Dislocation storage activities of nanoscale Al and Al-4Cu during tensile loading. **(a)** Dislocation structure evolution in tensile deformation of nanoscale Al with $D = 200$ nm. A large number of dislocations stick at the sample edge due to the native Al oxide shell then suddenly disappear after fracture. **(b)** Dislocation structure evolution in tensile deformation of nanoscale Al-4Cu with $D = 118$ nm. Efficient dislocations storage both around the shear-resistant precipitates and at the interface of the native Al oxide shell. Profuse dislocations were remained even after fracture.

nanoscale Al-4Cu can be quantified according to the Considére's criteria, $\sigma_f = \left(\frac{\partial\sigma}{\partial\varepsilon}\right)_{\dot{\varepsilon}}$, as plotted in Fig. 5 together with the total fracture strain. In general, the uniform elongation of nanoscale Al-4Cu ranges from ~5% to ~14% for different sample sizes, which overlaps with the uniform elongation of bulk Al-4Cu (around 6%) [28], as marked in Fig. 5. The fracture strain of nanoscale Al-4Cu is slightly higher than the uniform elongation but demonstrates a similar trend. In general, the smaller samples have uniform elongation comparable to the bulk counterpart, while the larger samples show slightly better uniform elongation, but with larger scatter. Overall, the uniform elongation of nanoscale Al-4Cu does not demonstrate a strong size-dependent behavior.

In contrast, the nanoscale Al-4Cu displays size-dependent fracture. As shown in Fig. 5, a transition from ductile to brittle fracture of nanoscale Al-4Cu can be evidenced. The nanoscale Al-4Cu with $D = 733$ nm shows obvious necking deformation before fracture. High density of dislocation debris appeared at the fracture front, and the fracture planes are roughly perpendicular to the loading axis. Notably, the fractured native Al oxide shell can be easily found at the fracture front, as marked in Fig. 5. With reducing the dimension, a transition from ductile fracture (necking) to brittle fracture happens, as seen in the samples with $D = 383$ nm and $D = 272$ nm in Fig. 5. The fracture of these samples can be divided into two parts: the brittle fracture of native Al oxide shell and the ductile fracture of the Al-4Cu matrix. With further reducing the sample size, a pure brittle fracture appeared, as shown for the sample with $D = 191$ nm in Fig. 5 and Movies S4. During tensile test, plenty of dislocations were operating along with straining, and accumulating around the θ' precipitates and at the edges. Surprisingly, the sample showed almost no necking stage and fractured catastrophically, forming a fracture surface perpendicular to the loading axis (Movie S4). In general, sudden brittle fracture was the typical fracture character of nanoscale Al-4Cu samples with D around 100 nm, necking dominated fracture in samples with $D > 600$ nm, and a mixture of brittle oxide shell failure and ductile matrix fracture took place in the medium sized range. These observations indicate that the earlier fracture of native oxide shell plays a role of precursor for the final fracture of nanoscale Al-4Cu.

Supplementary video related to this article can be found at http://dx.doi.org/10.1016/j.actamat.2016.12.055.

4. Discussion

The nanoscale Al-4Cu shows stable plastic flow and size-dependent strengthening, strain hardening and fracture, which are likely resulting from the effect of the native Al oxide shell. All tensile samples are covered with a layer of native Al oxide shell with a nearly constant thickness of $< t > \sim 4.3$ nm. Hence the volume fraction of native Al oxide shell for tensile samples can be determined, as plotted in Fig. 6a. Obviously, the volume fraction of oxide shell is only ~3% for $D = 700$ nm, and increased to ~20% for the sample with $D = 100$ nm, which will significantly enhance the mechanical performance of nanoscale Al-4Cu. In general, the smaller sample has a higher volume fraction of the native Al oxide shell. A relation between volume fraction of oxide shell and sample size can be observed by fitting the data in Fig. 6a, in the form of $f_{oxide} = 54.94D^{-1.2}$.

4.1. Modeling the size-dependent yield strength

The size-dependent yield strength observed in nanoscale Al-4Cu is unexpected, since the micron or sub-micron sized pillars with internal particles usually exhibit weak or no size effect [19–22]. Only those samples with extremely small sizes would exhibit obvious size effect, corresponding to a transition from particle spacing controlled deformation (size-independent) to dislocation source size dominated deformation (size-dependent) [23]. In the nanoscale Al-4Cu, the θ' precipitate spacing is constant ($\lambda_{ppt} \sim 87$ nm) [28], thus there should be no size effect in the large sample range, and a critical sample size of $D_c = 250$ nm is determined according to Fig. 3. Hence, for stage I in Fig. 3, the observed

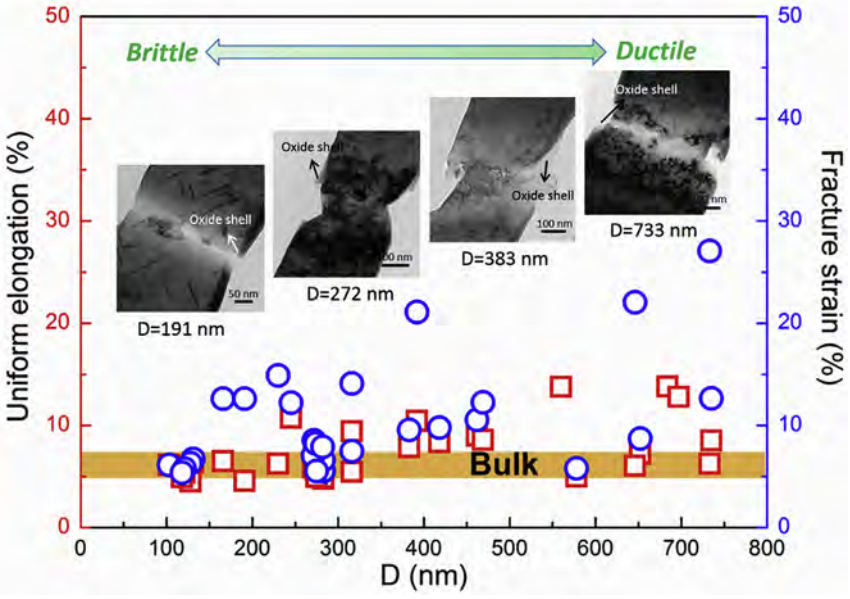

Fig. 5. The uniform elongation, fracture strain and ductile to brittle fracture transition of nanoscale Al-4Cu with reducing sample size. The uniform elongation and fracture strain of nanoscale Al-4Cu show weak size-dependent behavior. The uniform elongation of bulk Al-4Cu are labelled by the yellow band. The fracture behaviors demonstrated a clear transition from ductile deformation with necking ($D = 733$ nm), to a mixed brittle failure of oxide shell and necking of matrix ($D = 383$ nm and $D = 272$ nm), then to a complete brittle fracture of whole sample ($D = 191$ nm), as displayed by the inserted TEM images. (For interpretation of the references to colour in this figure legend, the reader is referred to the web version of this article.)

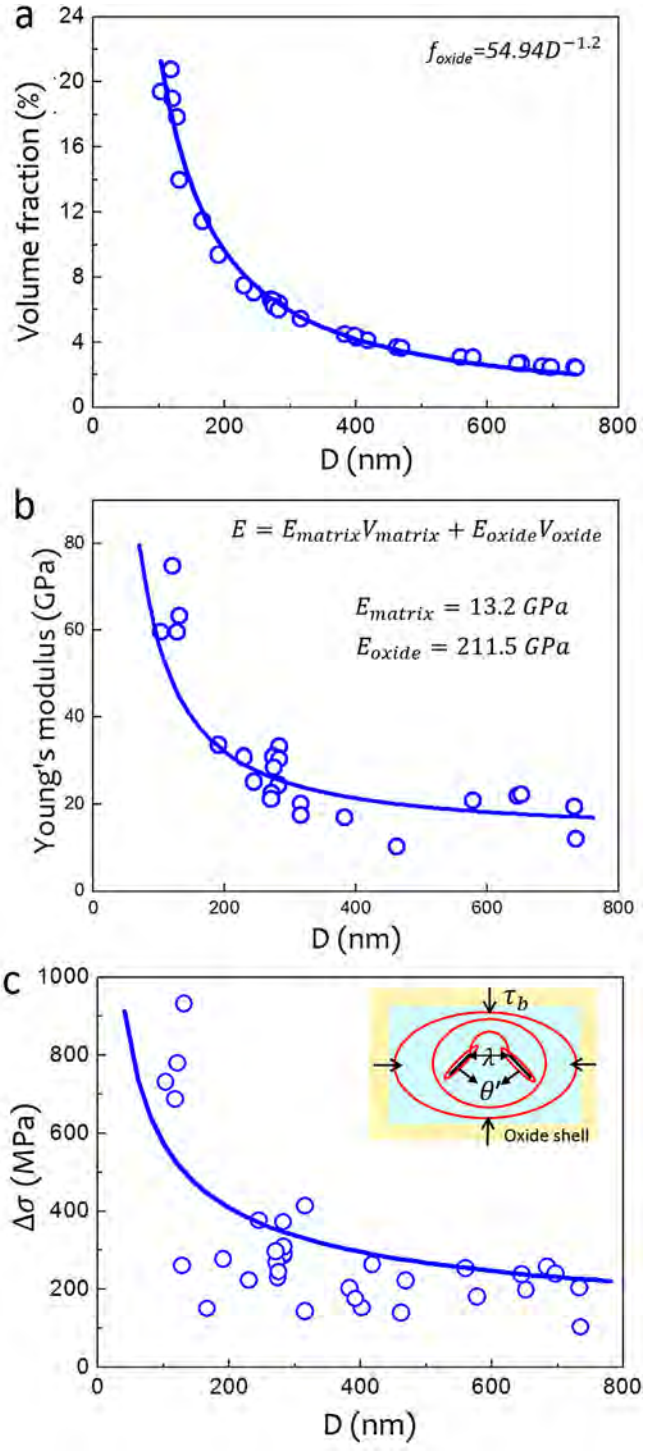

Fig. 6. Size-dependent volume fraction of native Al oxide shell, Young's modulus and model prediction of strain hardening. **(a)** The variation of volume fracture of native Al oxide shell with the sample size; **(b)** The size-dependence of Young's modulus of nanoscale Al with native oxide shell. The rule of mixture is valid for Young's modulus calculation during the elastic loading stage of nanosale Al alloy with native oxide. **(c)** Modeling the unprecedented strain hardening according to dislocation-precipitates and dislocation-oxide shell interactions.

size effect is mainly resulting from the variation of the volume fraction of native Al oxide shell. Hence the rule of mixtures can be used to compute the yield strength of native oxide shell and the Al-4Cu matrix, using

$$\sigma_Y = \sigma_{matrix} f_{matrix} + \sigma_{oxide} f_{oxide} \quad (1)$$

where σ_Y is the yield strength of nanoscale Al-4Cu, σ_{matrix} and σ_{oxide} are the yield strength of the matrix and the native Al oxide shell, f_{matrix} and f_{oxide} are volume fractions of the matrix and the native oxide shell, respectively. In order to check whether the rule of mixture is valid or not, the variation of Young's modulus with sample size for nanoscale Al with native oxide shell have been plotted in Fig. 6b and fitted by using the rule of mixture formula (see inset in Fig. 6b). It can be seen that the rule of mixture can be accurately predict the variation of Young's modulus of nanoscale Al with the sample size. The acquried modulus of Al oxide shell (211.5 GPa) is consistent well with previous experimental study [34]. These analyses indicate that the rule of mixture works for estimation of individual yield strength of Al matrix and oxide shell for nanoscale Al-4Cu samples.

According to the stage I size dependent strengthening, the estimated yield strength of native Al oxide shell is $\sigma_{oxide} \approx 3.85$ GPa , indicating the ultrahigh strength of the amorphous Al oxide shell. This estimation is consistent with some previous studies on the yield strength of amorphous Al oxide shell [33,34]. The calculated yield strength of Al-4Cu matrix is 320 MPa, which is very close to the yield strength of bulk Al-4Cu [28]. Due to the ultrahigh strength of native Al oxide shell, a mild increase of their volume fraction with reducing sample size will elevate the yield strength significantly, thus showing some extent of size-dependence, as shown in Figs. 2c and 3a. Once D < 250 nm, the yield strength of Al-4Cu displays a stronger size-dependence, which is caused by both the dislocation source size dominated deformation and the quick increase of the volume fraction of native Al oxide shell. Therefore the variation of yield strength of Al-4Cu with sample size can be modelled in the following:

For D > 250 nm, the precipitate spacing controls the deformation, and the size effect is mainly resulting from the variation of the volume fraction of native Al oxide shell, thus [28,29],

$$\sigma_Y = \left[\sigma_1 + \frac{m_0 Gb}{2\pi\sqrt{1-\nu}\lambda_{ppt}} \ln\left(\frac{r_o}{r_i}\right)\right] f_{matrix} + \sigma_{oxide}(D) f_{oxide} \quad (2)$$

where σ_1 is the sum of intrinsic lattice strength and the solid solution strength, m_0 is an orientations factor and can be determined by fitting stage I in Fig. 3a, such as $m_0 = 3.35$, λ_{ppt} is the average precipitate spacing (~87 nm) of peak aged Al-4Cu alloy [28]. The precipitate strengthening is calculated according to the Orowan model [29]. All the others symbols have the usual meaning.

For D < 250 nm, both the dislocation source size dominated deformation and the increasing of the volume fraction of native Al oxide shell give rise to the size effect, thus,

$$\sigma_Y = \left[\sigma_1 + \frac{m_0 Gb}{2\pi(1-\nu)\beta D} \ln\left(\frac{r_o}{r_i}\right)\right] f_{matrix} + \sigma_{oxide}(D) f_{oxide} \quad (3)$$

where βD is the size of dislocation source, and β is a scaling factor between dislocation source size and the dimension of sample [23]. Once the dislocation source size dominated strength become equals to the average precipitate spacing controlled strength, it is corresponding to the critical sample dimension for transition from stage I to stage II in Fig. 3a. Taking the critical size for transition, D_c = 250 nm, and the average spacing of precipitates in Al-4Cu, $\lambda_{ppt} \approx 87$ nm, thus a value of $\beta = 0.486$ can be obtained. We adopt r_i = b and $r_o = 3.5h^3$ for stage I and $r_o = \lambda_{ppt}$ for stage II, where h is the average thickness of the precipitates, hence the variation of yield strength of nanoscale Al-4Cu with the sample dimension can be well predicted, as shown in Fig. 2c.

4.2. Modeling the size-dependent strain hardening

Besides the anomalous size-dependent yielding, the strain hardening of nanoscale Al-4Cu also displays significant size effect, as shown in Fig. 2a and b. The strain hardening of nanoscale Al-4Cu mainly comes from two parts: kinematic hardening by the θ' precipitates and native oxide shell, and isotropic hardening by dislocations accumulated during straining. The θ' precipitates contribute to the kinematic hardening via forming high density of Orowan loops, which produce back stress on further slip of coming dislocations [28,29]. However, the magnitude of θ' precipitate kinematic hardening only depends on the volume fraction of precipitates, which is constant in current study, and a magnitude of ~ 40 MPa for precipitate kinematic hardening can be estimated according to previous experimental measurement [29]. Therefore the θ' precipitate induced kinematic hardening should be size-independent. Notably, the fully dense native oxide shell can suppresses the annihilation of dislocations at the free surface and block their slipping, leading to a rapid increase of dislocation density inside the tensile sample. The native oxide shell exerts a strong back stress on further coming dislocations as well, which also produces significant kinematic hardening. The oxide shell kinematic hardening and dislocation isotropic hardening should be size-dependent. With the operation of the above mechanisms, the magnitude of strain hardening contributed by the native Al oxide shell can be estimated as [35,36],

$$\Delta\tau_{B-oxide} = \frac{GNbcos\theta}{\pi(1-\nu)D} \tag{4}$$

where N is the number of dislocations accumulated on the slip plane, D is the dimension of the sample, and θ is the angle between the slip plane normal and the loading axis. The number of dislocations that can be stored inside the nanoscale Al-4Cu is highly dependent on the shear strength of the native Al oxide (Figs. 4 and 5) and the sample size. According to the stressed single pileup model [35], the maximum number of dislocations that can be storage on single slip plane is,

$$N = \sqrt{\frac{\pi(1-\nu)D\Delta\tau_{oxide}}{Gbcos\theta}} \tag{5}$$

where $\Delta\tau_{oxide}$ is the additional shear stress that the native Al oxide shell can sustain during strain hardening, and approximately $\Delta\tau_{oxide} = \frac{\sigma_{oxide}}{2} - \frac{\sigma_{oxide}}{m_0} - \tau_i$, where $\tau_i \approx \frac{Gb}{4\pi(1-\nu)<t>}$ is the image force [35]. Therefore the magnitude of back stress provided by the native oxide shell can be expressed as,

$$\Delta\tau_{B-oxide} = \sqrt{\frac{Gbcos\theta\Delta\tau_{oxide}}{\pi(1-\nu)D}}. \tag{6}$$

Hence the total strain hardening of nanoscale Al-4Cu can be estimated as:

$$\Delta\sigma = m_0\alpha Gb\sqrt{\rho} + m_0\Delta\tau_{B-oxide} + <\sigma>_{ppt} \tag{7}$$

here m_o is an orientation factor as introduced in Eq. (2), α is a constant in the range of 0.1–0.5 (0.15 is used in this work), and $\rho = Ncos\theta/D^2$ is the accumulated dislocation density [35]. Thus the total strain hardening of nanoscale Al-4Cu is highly size-dependent. The amount of strain hardening reflected by the difference between UTS and yield strength, $\Delta\sigma$, is plotted with sample dimension, in comparison with the modeling (Fig. 6c). To facilitate the estimation of the ultimate strain hardening of Al-4Cu sample, we assume the dislocations are accumulated mainly on one slip plane, and such calculation will overestimate the dislocation density, which is likely part of the reason why the prediction in Fig. 6c is slightly higher than the experimental data. The physical model captures the general trend of size-dependent strain hardening of nanoscale Al-4Cu, and the kinematic hardening produced by ultrathin native oxide shell provides the largest fraction of strain hardening in comparison with the precipitate kinematic hardening and dislocation isotropic hardening. In general, with reducing the sample dimension, the dislocations have a higher chance to interact with the native Al oxide shell directly. Hence the catastrophic fracture of nanoscale Al-4Cu with size of 100 nm was mainly caused by the earlier failure of the native oxide shell, then the matrix was overloaded, and lead to brittle fracture morphology, as shown in Fig. 5. The above analyses indicate that an intact ultrathin native oxide shell plays a decisive role in achieving the extraordinary mechanical properties of nanoscale Al-4Cu alloys.

Fig. 7a plots the toughness/Young's modulus versus the UTS/Young's modulus of nanoscale Al-4Cu alloys, in comparison with the tensile data of other bulk and nanoscale metals [37–48]. This normalized plot highlights the unprecedented mechanical properties of nanoscale Al-4Cu resulting from its unique core-shell composite structure. The corresponding UTS/Young's modulus versus ductility plot is shown in Fig. 7b. It is obvious that the nanoscale Al-4Cu alloys with ultrathin native oxide shell have the best combination of toughness and UTS or UTS and ductility,

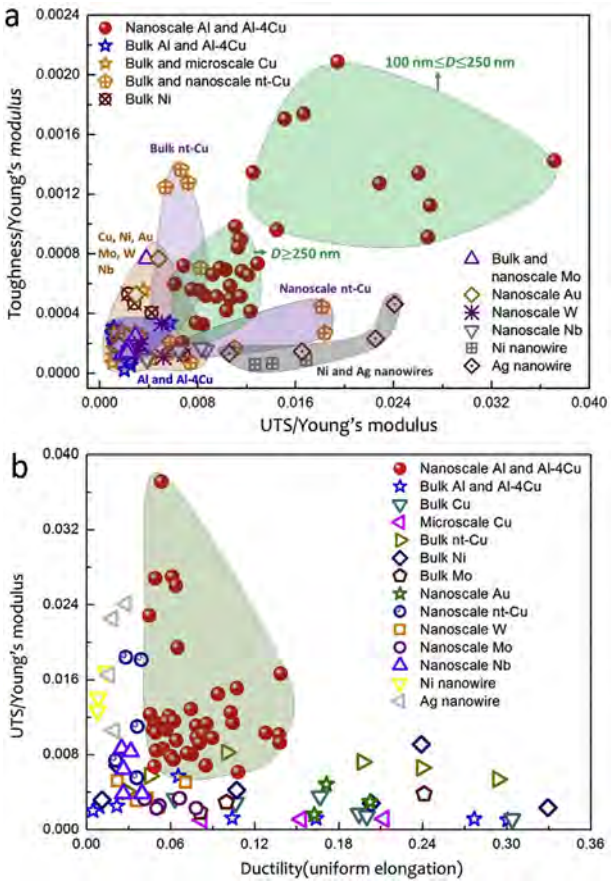

Fig. 7. Ashby map showing the toughness/Young's modulus versus ultimate tensile strength (UTS)/Young's modulus **(a)** and ultimate tensile strength (UTS)/Young's modulus versus ductility **(b)** plot of nanoscale Al and Al-4Cu and in comparison with other bulk or nanoscale metals [37–48]. The nanoscale Al-4Cu alloys have the unprecedented combination of toughness and UTS or UTS and ductility. The toughness is measured from the area covered by the true stress-strain curves.

especially for samples with D < 250 nm, which reside in an unprecedented regime for metals [37–48]. Therefore the ultrathin native oxide covered nanoscale metals are likely to be useful and should be further explored in future.

5. Conclusions

We found a new strategy to combine strengthening and plastic stability for small-volume metals. A nanoscale Al-4Cu with an ultrathin native oxide shell, as long as the latter remains intact, demonstrates size strengthening as well as proficient strain hardening that suppresses plastic instability to deliver bulk-like tensile ductility and toughness. The overall mechanical stability and performance is unprecedented for known bulk and nanoscale metals, as reflected in the normalized strength-toughness plot. Our findings bring attention to the potential benefits of a thin and dense native oxide, such as alumina, silica and chromia, in enabling strengthening concomitant with efficient dislocation storage. This approach may find practical use in micro- and nano-systems, to produce deformation-friendly metallic structures and devices.

Acknowledgements

This work was supported by the National Natural Science Foundation of China (Grant Nos.51471128, 51231005, 51321003). W.Z.H. would like to thank the support of Youth Thousand Talents Program of China and the Young Talent Support Plan of XJTU. J.L. acknowledges support by NSF DMR-1410636 and DMR-1120901. S.H.L appreciates M.S.D for the kind assistance during the earlier stage of this project.

References

[1] J.R. Greer, J.T.M. De Hosson, Plasticity in small-sized metallic systems: intrinsic versus extrinsic size effect, Prog. Mater. Sci. 56 (2011) 654–724.
[2] M.D. Uchic, D.M. Dimiduk, J.N. Florando, W.D. Nix, Sample dimensions influence strength and crystal plasticity, Science 305 (2004) 986–990.
[3] J.R. Greer, W.C. Oliver, W.D. Nix, Size dependence of mechanical properties of gold at the micro scale in the absence of strain gradients, Acta Mater. 53 (2005) 1821–1830.
[4] K.S. Ng, A.H.W. Ngan, Stochastic nature of plasticity of aluminum micro-pillars, Acta Mater. 56 (2008), 1721–1720.
[5] H. Bei, S. Shim, G.M. Pharr, E.P. George, Effects of pre-strain on the compressive stress-strain response of Mo-alloy single-crystal micropillars, Acta Mater. 56 (2008) 4762–4770.
[6] J.R. Greer, W.D. Nix, Nanoscale gold pillars strengthened through dislocation starvation, Phys. Rev. B 73 (2006) 245410.
[7] Z.W. Shan, R.K. Mishra, S.A.S. Asif, O.L. Warren, A.M. Minor, Mechanical annealing and source-limited deformation in submicrometer-diameter Ni crystals, Nat. Mater. 7 (2008) 115–119.
[8] S.I. Rao, D.M. Dimiduk, T.A. Parthasarathy, M.D. Uchic, M. Tang, C. Woodward, Athermal mechanisms of size-dependent crystal flow gleaned from three-dimensional discrete dislocation simulations, Acta Mater. 56 (2008) 3245–3259.
[9] S.H. Oh, M. Legros, D. Kiener, G. Dehm, In situ observation of dislocation nucleation and escape in a submicrometre aluminium single crystal, Nat. Mater. 8 (2009) 95–100.
[10] D. Kiener, A.M. Minor, Source truncation and exhaustion: insights from quantitative in situ TEM tensile testing, Nano Lett. 11 (2011) 3816–3820.
[11] Z.J. Wang, Q.J. Li, Z.W. Shan, J. Li, J. Sun, E. Ma, Sample size effects on the large strain bursts in submicron aluminum pillars, Appl. Phys. Lett. 100 (2012) 0719906.
[12] F. Mompious, M. Legros, A. Sedlmayr, D.S. Gianola, D. Caillard, O. Kraft, Source-based strengthening of sub-micrometer Al fibers, Acta Mater. 60 (2012) 977–983.
[13] A. Kunz, S. Pathak, J.R. Greer, Size effects in Al nanopillars: single crystalline vs. bicrystalline, Acta Mater. 59 (2011) 4416–4424.
[14] D.C. Jang, C. Cai, J.R. Greer, Influence of homogeneous interfaces on the strength of 500 nm diameter Cu nanopillars, Nano Lett. 11 (2011) 1743–1746.
[15] Z.J. Wang, Z.W. Shan, J. Li, J. Sun, E. Ma, An index for deformation controllability of small-volume materials, Sci. China Tech. Sci. 57 (2014) 663–670.
[16] L.L. Li, Z.J. Zhang, J. Tan, C.B. Jiang, R.T. Qu, P. Zhang, J.B. Yang, Z.F. Zhang, Stepwise work hardening induced by individual grain boundary in Cu bicrystal micropillars, Sci. Rep. 5 (2015) 15631.
[17] N.A. Mara, D. Bhattacharyya, J.P. Hirth, P. Dickerson, A. Misra, Mechanism for shear banding in nanolayered composites, Appl. Phys. Lett. 97 (2010) 021909.
[18] J.Y. Zhang, G. Liu, J. Sun, Self-toughening crystalline Cu/amorphous Cu-Zr nanolaminates: deformation-induced devitrification, Acta Mater. 66 (2014) 22–31.
[19] X.L. Guo, Q. Guo, Z.Q. Li, G.L. Fan, D.B. Xiong, Y.S. Su, J. Zhang, C.L. Gan, D. Zhang, Interfacial strength and deformation mechanism of SiC-Al composites micro-pillars, Scr. Mater. 114 (2016) 56–59.
[20] B. Girault, A.S. Schneider, C.P. Frick, E. Arzt, Strength effects in micropillars of a dispersion strengthened superalloy, Adv. Eng. Mater. 12 (2010) 385–388.
[21] R. Gu, A.H.W. Ngan, Size effect on the deformation behavior of duralumin micropillars, Scr. Mater. 68 (2013) 861–864.
[22] T. Hu, L. Jiang, H. Yang, K.K. Ma, T.D. Topping, J.S. Yee, M.J. Li, A.K. Mukherjee, J.M. Schoenung, E.J. Lavernia, Stabilized plasticity in ultrahigh strength, sub-micro Al crystals, Acta Mater. 94 (2015) 46–58.
[23] D. Kiener, P. Hosemann, S.A. Maloy, A.M. Minor, In situ nanocompression testing of irradiated copper, Nat. Mater. 10 (2011) 608–613.
[24] N. Li, N.A. Mara, Y.Q. Wang, M. Nastasi, A. Misra, Compressive flow behavior of Cu thin films and Cu/Nb multilayers containing nanometer-scale helium bubbles, Scr. Mater. 64 (2011) 974–977.
[25] M.S. Ding, J.P. Du, L. Wan, S. Ogata, L. Tian, E. Ma, W.Z. Han, J. Li, Z.W. Shan, Radiation-induced helium nanobubbles enhance ductility in submicron-sized single crystalline copper, Nano Lett. 16 (2016) 4118–4124.
[26] K.S. Ng, A.H.W. Ngan, Effects of trapping dislocations within small crystals on their deformation behavior, Acta Mater. 57 (2009) 4902–4910.
[27] A.T. Jennings, C. Gross, F. Greer, Z.H. Aitken, S.-W. Lee, C.R. Weinberger, J.R. Greer, Higher compressive strengths and the Bauschinger effect in conformally passivated copper nanopillars, Acta Mater. 60 (2012) 3444–3455.
[28] W.Z. Han, A. Vinogradov, C.R. Hutchinson, On the reversibility of dislocation slip during cyclic deformation of Al alloys containing shear-resistant particles, Acta Mater. 59 (2011) 3720–3736.
[29] J.D. Teixeira, L. Bourgeois, C.W. Sinclair, C.R. Hutchinson, The effect of shear-resistant, plate-shaped precipitates on the work hardening of Al alloys: towards a prediction of the strength–elongation correlation, Acta Mater. 57 (2009) 6075–6089.
[30] L. Bourgeois, C. Dwyer, M. Weyland, J.F. Nie, B.C. Muddle, Structure and energetics of the conherent interface between the theta prime precipitate phase and aluminum in Al-Cu, Acta Mater. 59 (2011) 7043–7050.
[31] A. Bianconi, Al-Al2O3 interface study using surface soft-x-ray absorption and photoemission spectroscopy, Phys. Rev. B 19 (1979) 2837–2843.
[32] F.G. Sen, A.T. Alpas, A.C.T. Duin, Y. Qi, Oxidation-assisted ductility of aluminium nanowires, Nat. Commun. 5 (2014) 3959.
[33] D.G. Xie, Z.J. Wang, J. Sun, J. Li, E. Ma, Z.W. Shan, In situ study of the initiation of hydrogen bubbles at the aluminium metal/oxide interface, Nat. Mater. 14 (2015) 899–904.
[34] K. Tapily, J.E. Jakes, D.S. Stone, P. Shrestha, D. Gu, H. Baumgart, A.A. Elmustafa, Nanoindentation investigation of HfO_2 and Al_2O_3 films grown by atomic layer desposition, J. Elect. Soc. 155 (2008) H545–H551.
[35] J.P. Hirth, J. Lothe, Theory of Dislocations, Krieger publishing company Malabar, Florida, 1982, p. p764.
[36] Y.N. Cui, Z.L. Liu, Z. Zhuang, Theoretical and numerical investigations on confined plasticity in micropillars, J. Mech. Phys. Solids 76 (2015) 127–143.
[37] C.Y. Yu, P.W. Kao, C.P. Chang, Transition of tensile deformation behaviors in ultrafine-grained aluminum, Acta Mater. 53 (2005) 4019–4028.
[38] D. Kiener, M. Rester, S. Scheriau, B. Yang, R. Pippan, G. Dehm, Influence of external and internal length scale on the flow stress of copper, Int. J. Mater. Res. 98 (2007) 1047–1053.
[39] L. Lu, Y.F. Shen, X.H. Chen, L.H. Qian, K. Lu, Ultrahigh strength and high electrical conductivity in copper, Science 304 (2004) 422–426.
[40] L. Lu, X. Chen, X. Huang, K. Lu, Revealing the maximum strength in nanotwinned copper, Science 323 (2009) 607–610.
[41] J.Y. Kim, J.R. Greer, Tensile and compressive behavior of gold and molybdenum single crystals at the nano-scale, Acta Mater. 57 (2009) 5245–5253.
[42] J.Y. Kim, D.C. Jang, J.R. Greer, Tensile and compressive behavior of tungsten, molybdenum, tantalum and niobium at the nanoscale, Acta Mater. 58 (2010) 2355–2363.
[43] D.C. Jang, X.Y. Li, H.J. Gao, J.R. Greer, Deformation mechanisms in nanotwinned metal nanopillars, Nat. Nanotechnol. 7 (2012) 594–601.
[44] G. Liu, G.J. Zhang, F. Jiang, X.D. Ding, Y.J. Sun, J. Sun, Nanostructured high-strength molybdenum alloys with unprecedented tensile ductility, Nat. Mater. 12 (2013) 344–350.
[45] C. Peng, Y. Zhong, Y. Lu, S. Narayanan, T. Zhu, J. Lou, Strain rate dependent mechanical properties in single crystal nickel nanowires, Appl. Phys. Lett. 102 (2013) 083102.
[46] S. Narayanan, G.M. Cheng, Z. Zeng, Y. Zhu, T. Zhu, Strain hardening and size effect in five-fold twinned Ag nanowires, Nano Lett. 15 (2015) 4037–4044.
[47] X.L. Wu, F.P. Yuan, M.X. Yang, P. Jiang, C.N. Zhang, L. Chen, Y.G. Wei, E. Ma, Nanodomained nickel unite nanocrystal strength with coarse-grain ductility, Sci. Rep. 5 (2015) 11728.
[48] R. Ramachandramoorthy, W. Gao, R. Bernal, H. Espinosa, High strain rate tensile testing of silver nanowires: rate-dependent brittle-to-ductile transition, Nano Lett. 16 (2016) 255–263.